

RESEARCH PAPER



ATG7 is essential for secretion of iron from ameloblasts and normal growth of murine incisors during aging

Supawadee Sukseree ^a, Uwe Yacine Schwarze ^b, Reinhard Gruber ^b, Florian Gruber ^a, Maria Quiles Del Rey^c, Joseph D. Mancias^c, John D. Bartlett ^d, Erwin Tschachler ^a, and Leopold Eckhart ^a

^aResearch Division of Biology and Pathobiology of the Skin, Department of Dermatology, Medical University of Vienna, Vienna, Austria;

^bDepartment of Oral Biology, Medical University of Vienna, Vienna, Austria; ^cDivision of Genomic Stability and DNA Repair, Department of Radiation Oncology, Dana-Farber Cancer Institute, Boston, MA, USA; ^dDivision of Biosciences, College of Dentistry, The Ohio State University, Columbus, OH, USA

ABSTRACT

The incisors of rodents comprise an iron-rich enamel and grow throughout adult life, making them unique models of iron metabolism and tissue homeostasis during aging. Here, we deleted *Atg7* (autophagy related 7) in murine ameloblasts, i.e. the epithelial cells that produce enamel. The absence of ATG7 blocked the transport of iron from ameloblasts into the maturing enamel, leading to a white instead of yellow surface of maxillary incisors. In aging mice, lack of ATG7 was associated with the growth of ectopic incisors inside severely deformed primordial incisors. These results suggest that 2 characteristic features of rodent incisors, i.e. deposition of iron on the enamel surface and stable growth during aging, depend on autophagic activity in ameloblasts.

Abbreviations: ATG5: autophagy related 5; ATG7: autophagy related 7; CMV: cytomegalovirus; Cre: Cre recombinase; CT: computed tomography; FTH1: ferritin heavy polypeptide 1; GFP: green fluorescent protein; KRT5: keratin 5; KRT14: keratin 14; LGALS3: lectin, galactose binding, soluble 3; MAP1LC3/LC3: microtubule-associated protein 1 light chain 3; NCOA4: nuclear receptor coactivator 4; NRF2: nuclear factor, erythroid 2 like 2; SQSTM1: sequestosome 1.

ARTICLE HISTORY

Received 18 March 2019
Revised 11 November 2019
Accepted 18 December 2019

KEYWORDS

Aging; ameloblast; ATG7; autophagy; epithelium; ferritin; hyperplasia; iron; secretion; tooth

Introduction

Tooth development and growth is driven by specialized epithelial and mesenchymal cells. The hard surface layer of teeth, i.e. the enamel, is formed by epithelial cells named ameloblasts. Initially, ameloblasts secrete proteins to form an organic matrix and calcium ions to establish a partially mineralized enamel. Subsequently, ameloblasts secrete proteases that cleave enamel matrix proteins and allow the completion of enamel mineralization so that the calcium hydroxyphosphate (hydroxyapatite) content reaches 95% in mature enamel [1,2]. In rodent incisors, particularly of the upper jaw (maxilla) (Figure 1A), the maturation of the enamel includes a pigmentation stage during which ameloblasts deposit iron in the outermost layer of the enamel [3–5], resulting in yellow color of the enamel. The iron content of the outermost micrometers on the labial side of rodent incisors exceeds 5% [6]. The mechanism of iron secretion has remained incompletely understood, however, high expression levels of ferritin in rodent ameloblasts are likely to play a critical role in this unique transport of iron [7]. In contrast to the development of most mammalian teeth, which is limited to early life, rodent incisors grow throughout adult life, thus making them a unique model system for studies of amelogenesis and aging.

Macroautophagy/autophagy is a subcellular process by which organelles, protein complexes, and soluble components of the cytoplasm are delivered to lysosomes for degradation [8–10]. This process is regulated and mediated by a set of proteins such as ATG5 (autophagy related 5), ATG7, MAP1LC3/LC3 (microtubule-associated protein 1 light chain 3), SQSTM1/p62 (sequestosome 1) and others. Inactivation of either ATG5 or ATG7 disrupts autophagic flux and global knockout of *Atg5* or *Atg7* genes in mice results in perinatal lethality [11]. However, deletion of these genes using the Cre-lox system and cell type-specific promoters to drive expression of Cre recombinase, allows for suppression of autophagy in post-natal life. Studies of such conditional knockout mice have demonstrated that autophagy is crucial for maintaining cellular homeostasis under starvation conditions and upon exposure to stress in various organ systems [11–13]. Despite great progress in our understanding of the contribution of autophagy to tissue homeostasis, the physiological functions of autophagy in many cell types have remained elusive.

To unravel roles of autophagy in the integumentary epithelium and its appendages, we have created mouse models in which essential autophagy genes are deleted in epithelial progenitor cells that express keratins KRT5 and KRT14 [13,14].

In *Atg5^{ff} Krt5-Cre* and *Atg7^{ff} Krt14-Cre* mice, all cells derived from KRT5- and KRT14-positive stem cells, including epidermal keratinocytes, thymic epithelial cells, Merkel cells and epithelial cells of sebaceous and sweat glands lack ATG5 and ATG7, respectively, and therefore do not activate autophagy [14–19].

Ameloblasts develop from KRT5/KRT14-positive precursor cells [20], and therefore *Atg5^{ff} Krt5-Cre* and *Atg7^{ff} Krt14-Cre* mice can be used to test the hypothesis that autophagy contributes to the homeostasis and function of the enamel epithelium. In the present study, we investigated mainly *Atg7^{ff} Krt14-Cre* mice and found that the genetic suppression of autophagy in epithelial cells impairs the secretion of iron into the enamel and leads to progressive odontoma-like malformations of maxillary incisors during aging.

Results

ATG7 facilitates the formation of GFP-LC3-labeled vesicles and prevents the accumulation of SQSTM1 in the murine enamel epithelium

To localize autophagic activity in the enamel epithelium *in vivo*, we studied transgenic mice that express green fluorescent protein (GFP) fused to MAP1LC3 (GFP-LC3) [21]. GFP-LC3 puncta, corresponding to autophagosomes or autophagosome-related vesicles, were readily detectable in ameloblasts of the maturation stage but not in the adjacent papillary layer of the enamel organ of the upper jaws (Figure 1B, D, arrows). *GFP-LC3 Atg7^{ff} Krt14-Cre* mice lacked a vesicular distribution of GFP-LC3 and rather showed diffuse accumulations of GFP-LC3 (Figure 1C, E, arrowheads), indicating that GFP-LC3-positive vesicles in ameloblasts required ATG7 for their formation.

To determine whether autophagy is necessary for protein homeostasis in ameloblasts, we investigated the abundance and distribution of the autophagy substrate, SQSTM1, in *Atg7^{ff} Krt14-Cre* mice [14,16] (Figure 1G–I) and, for control, fully autophagy-competent *Atg7^{ff}* mice (Figure 1F). Immunohistochemical analysis showed accumulation and aggregation of SQSTM1 in ameloblasts and papillary layer cells of *Atg7^{ff} Krt14-Cre* mice (Figure 1G, I) but not of *Atg7^{ff}* mice (Figure 1F), indicating that the autophagic degradation of this protein was impaired by the deletion of *Atg7* in the enamel epithelium. Together, the absence of GFP-LC3-labeled autophagosomes and the accumulation of SQSTM1 confirmed successful abrogation of ATG7-dependent processes in the enamel epithelium of *Atg7^{ff} Krt14-Cre* mice.

Krt14-Cre-induced deletion of ATG7 blocks the secretion of iron into the enamel and leads to growth of white instead of normal yellow incisors

The effect of epithelial *Atg7* deletion on teeth was determined by the inspection of more than 50 *Atg7^{ff} Krt14-Cre* and *Atg7^{ff}* (wild-type) mice. The labial side of the maxillary incisors of all wild-type mice was consistently yellow whereas the incisors of all *Atg7^{ff} Krt14-Cre* mice were aberrantly white (Figure 2A). The mandibular incisors were glassy white in *Atg7^{ff}* (wild type) mice and milky white in *Atg7^{ff} Krt14-Cre* mice but this phenotypic difference was

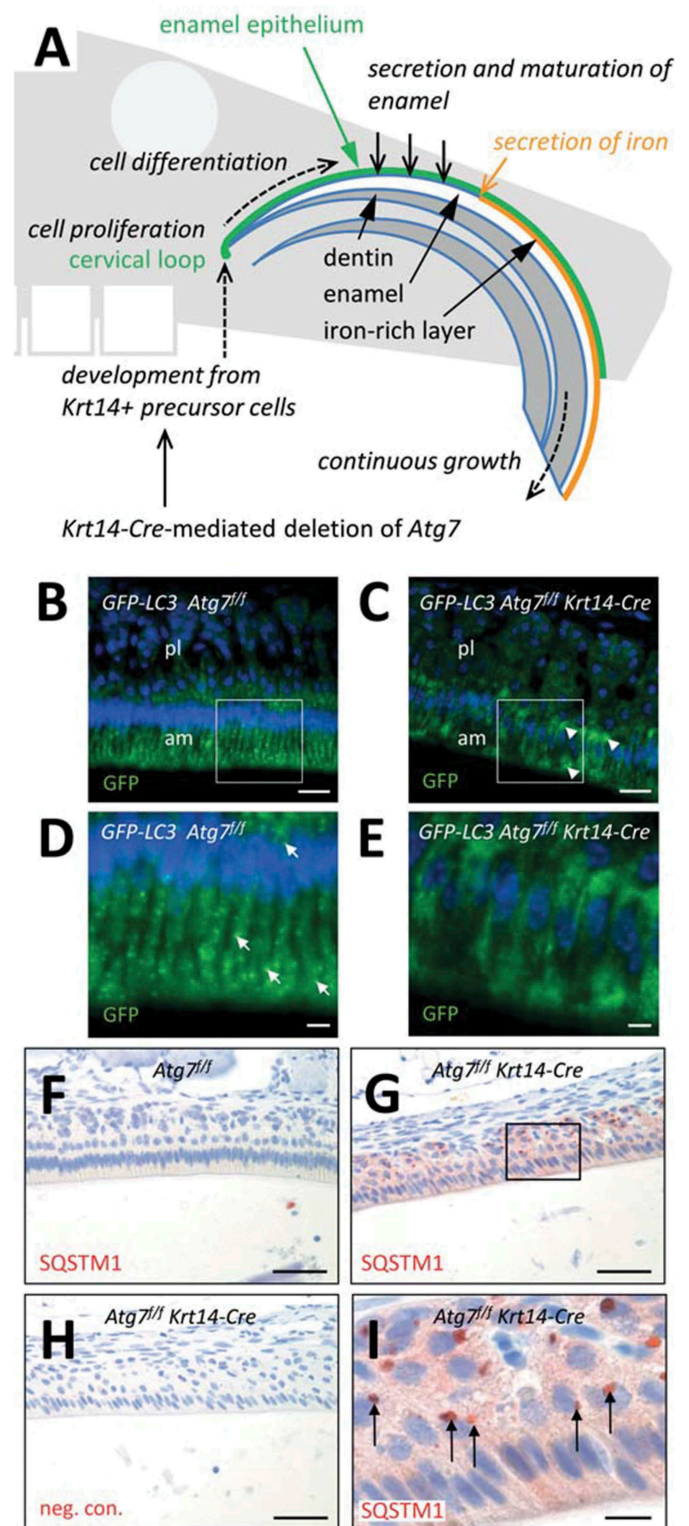


Figure 1. Suppression of autophagy in the enamel epithelium of *Atg7^{ff} Krt14-Cre* mice. (A) Schematic depiction of structure and growth of a murine maxillary incisor. Ameloblasts proliferate in the cervical loop and subsequently differentiate to produce enamel, including a superficial iron-rich layer. (B–E) The *Gfp-Lc3* transgene was introduced into *Atg7^{ff}* (B, D) and *Atg7^{ff} Krt14-Cre* (C, E) mice. Upper jaws were sectioned and immuno-labeled with anti-GFP (green). Nuclear DNA was labeled with Hoechst dye (blue). Panels D and E show higher magnifications of the boxed areas in panels B and C, respectively. Arrows in D mark GFP-LC3-positive vesicles. am, ameloblasts; pl, papillary layer. (F–I) Immunostaining of the autophagy substrate SQSTM1. Sections through the enamel organ of *Atg7^{ff}* (F) and *Atg7^{ff} Krt14-Cre* (G–I) mice were immunostained for SQSTM1 (red). A negative control staining of *Atg7^{ff} Krt14-Cre* tissue is shown in panel H. Scale bars: 20 μ m (B, C), 5 μ m (D, E), 50 μ m (F–H), 10 μ m (I).

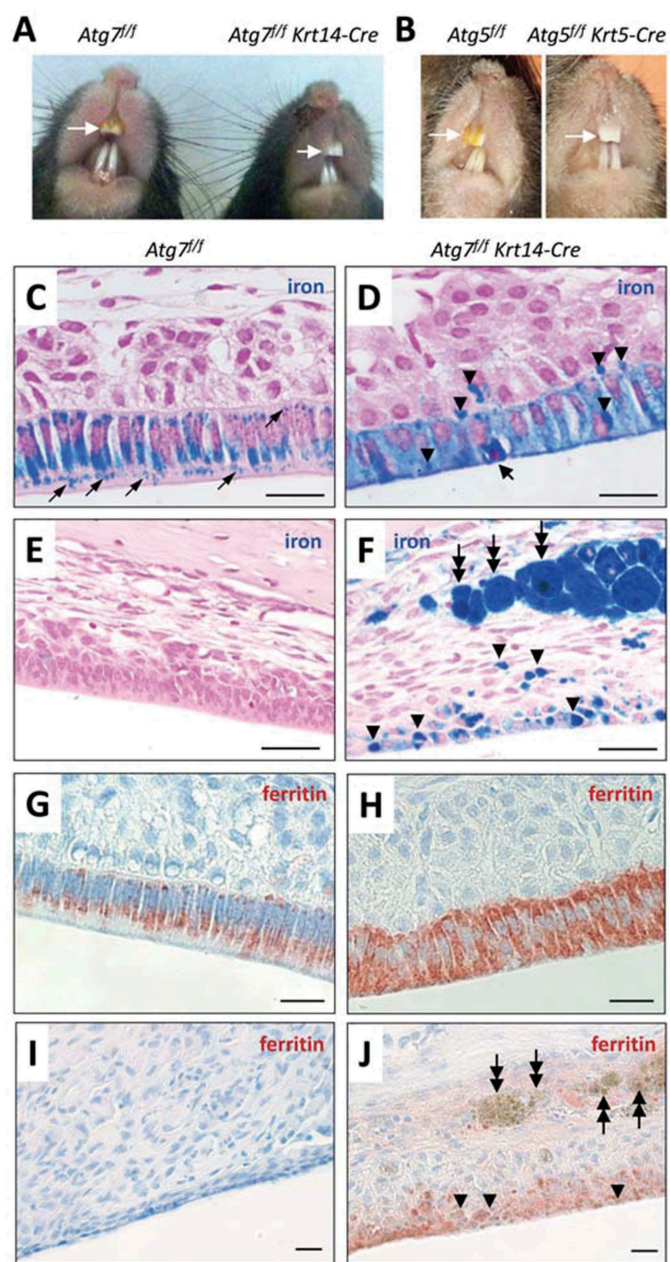


Figure 2. Ameloblasts of *Atg7^{fl/fl} Krt14-Cre* mice have a defect in iron secretion. (A) Comparison of incisor colors of an *Atg7^{fl/fl}* (fully autophagy-competent) and an *Atg7^{fl/fl} Krt14-Cre* (epithelial autophagy-deficient) mouse. (B) Comparison of incisors of an *Atg5^{fl/fl}* and an *Atg5^{fl/fl} Krt5-Cre* mouse. The maxillary incisors are marked by white arrows (A, B). (C–J) Sections through the enamel epithelium were stained with the iron-specific dye Perls' Prussian blue and counterstained with nuclear fast red (C–J) or immunostained for FTH1 (red) and counterstained with hematoxylin (blue) (G–J). Images show the pigmentation stage epithelium (C, D, G, H) and the distal epithelium (E, F, I, J). Thin arrows (C) indicate iron-containing vesicles. A thick arrow (D) indicates a condensed nucleus of an apoptotic ameloblast. Arrowheads (D, F, J) indicate accumulations of iron, and two-headed arrows (F, J) indicate iron-containing macrophages. Scale bars: 20 μ m (C–J).

less obvious. The molars of *Atg7^{fl/fl} Krt14-Cre* mice appeared normal in color and shape. Deletion of the autophagy gene *Atg5* in integumentary epithelial cells of *Atg5^{fl/fl} Krt5-Cre* mice also led to aberrantly decolorized incisors (Figure 2B), suggesting that the “pigmentation” of maxillary incisors required not only ATG7 but also ATG5. By contrast, deletion of the autophagy receptor gene

Sqstm1 did not impair yellow pigmentation of incisors (Fig. S1), indicating that SQSTM1 was not required for the secretion of iron. The further investigations were focused on the maxillary incisors of *Atg7^{fl/fl} Krt14-Cre* mice.

The yellow color of rodent incisors is caused by secretion of iron from ameloblasts and its deposition in the superficial layer of the enamel. As the enamel of *Atg7^{fl/fl} Krt14-Cre* incisors apparently lacked iron, we investigated the distribution of iron in the enamel organ. To this end, tissue sections were stained with the iron-specific dye Perls' Prussian blue. In *Atg7^{fl/fl}* mice, ameloblasts at the pigmentation stage contained high amounts of iron some of which appeared to be located in vesicles (Figure 2C). By contrast, *Atg7^{fl/fl} Krt14-Cre* ameloblasts of the pigmentation stage were diffusely stained blue and, in addition, contained darkly stained aggregations of iron (Figure 2D, arrowheads). A small portion of cells rich in iron showed a condensed nucleus indicating apoptosis (Figure 2D, thick arrow). Iron accumulations were present not only in ameloblasts but focally also in the papillary layer of *Atg7^{fl/fl} Krt14-Cre* mice (Figure 2D). *Atg7^{fl/fl}* ameloblasts did not contain iron in the latest stage of differentiation (Figure 2E), whereas iron deposits remained present in terminally differentiated *Atg7^{fl/fl} Krt14-Cre* ameloblasts (Figure 2F). In addition, strong iron accumulations were present in giant macrophages within the mesenchyme adjacent to the distal enamel epithelium of *Atg7^{fl/fl} Krt14-Cre* mice (Figure 2F, two-headed arrows). The high concentration of iron within macrophages and later stage ameloblast was readily visible even in hematoxylin and eosin-stained tissue sections of *Atg7^{fl/fl} Krt14-Cre* mice whereas no such iron deposits were present in autophagy-competent control mice (Fig. S2). The iron-binding protein ferritin was highly abundant in ameloblasts of the maturation stage in both and *Atg7^{fl/fl} Krt14-Cre* mice (Figure 2G, H), with an intracellular distribution equivalent to that of iron (Figure 2C, D). Ferritin disappeared in late-stage differentiated ameloblasts of *Atg7^{fl/fl}* mice (Figure 2I) but remained detectable in the distal enamel epithelium of *Atg7^{fl/fl} Krt14-Cre* mice (Figure 2J), though it was not or only weakly associated with iron deposits in epithelial cells and macrophages (Figure 2J; Figure S3). These results suggest that the deletion of *Atg7* impaired the secretion of iron into the enamel, leading to its retention in epithelial cells and later to its uptake and removal by macrophages.

Epithelial ATG7 is required for the normal maintenance of the cell growth compartment of murine incisors during aging

The difference between the yellow maxillary incisors of wild-type mice and their white counterparts of *Atg7^{fl/fl} Krt14-Cre* mice was stable throughout the observation period up to 2 years of age (Figure 3A). In *Atg7^{fl/fl} Krt14-Cre* mice older than 1.5 years, another phenotype became evident. Ninety one percent of the male and 42% of the female *Atg7^{fl/fl} Krt14-Cre* mice developed malformations and showed signs of damage of maxillary incisors whereas only 9% of the male and none of the female *Atg7^{fl/fl}* mice had abnormally shaped incisors ($n > 10$ for each group) (Figure 3A). The high rate of incisor malformations prompted us to further investigate these age-dependent changes of incisors in old *Atg7^{fl/fl} Krt14-Cre* mice.

When *Atg7^{fl/fl} Krt14-Cre* mice grew old, their maxillary incisors increased in width and formed labial grooves visible already on

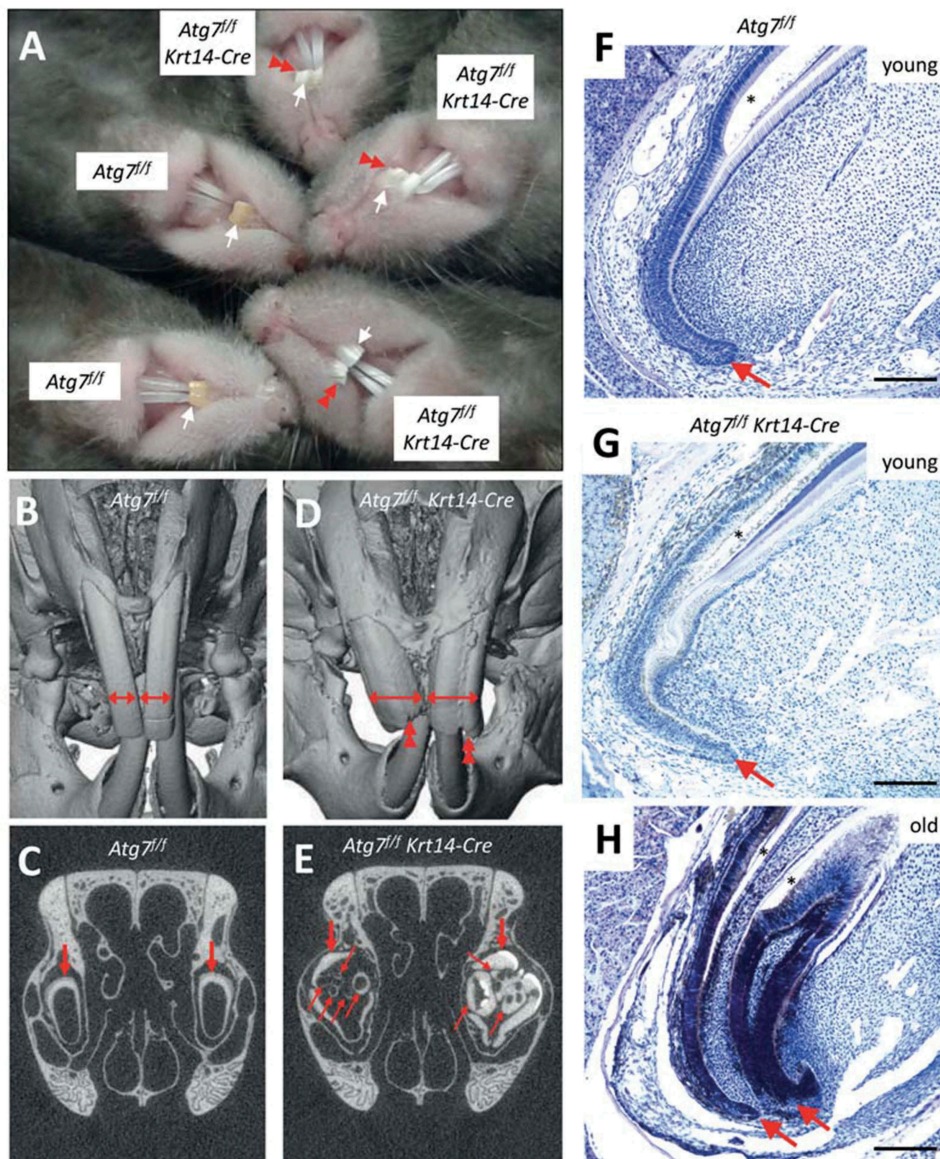


Figure 3. Inactivation of *Atg7* in epithelial cells leads to the development of malformations during the growth of maxillary incisors in *Atg7^{fl/fl} Krt14-Cre* mice. (A) Comparison of incisors of *Atg7^{fl/fl}* and *Atg7^{fl/fl} Krt14-Cre* mice aged over 1.5 years. The maxillary incisors are marked by white arrows. Red double arrowheads indicate malformations and damage of incisors of old *Atg7^{fl/fl} Krt14-Cre* mice. (B–E) The heads of old *Atg7^{fl/fl}* (24 months) and *Atg7^{fl/fl} Krt14-Cre* (22 months) mice were investigated by micro-computed tomography. Front view of *Atg7^{fl/fl}* (B) and *Atg7^{fl/fl} Krt14-Cre* (D) heads showed an aberrant increase in the width of maxillary incisors (horizontal double-headed arrows) and irregular damage (double arrowheads) at the apical ends of *Atg7^{fl/fl} Krt14-Cre* incisors. Frontal sections of micro-CT revealed that the incisors of *Atg7^{fl/fl}* mice (C) consisted of a single tube (thick arrow), representing the normal condition, whereas incisors of *Atg7^{fl/fl} Krt14-Cre* mice (E) contained additional incisor tubes (thin arrows). Micro-CT data are representative for $n = 3$ mice of each genotype. (F–H) Mice of different age (young: 1–2 months, old: 22 months) were sacrificed, the heads were fixed in formaldehyde, de-calcified and sagittal-sectioned. The tissue sections were subjected to hematoxylin and eosin staining. Young *Atg7^{fl/fl}* (F) and *Atg7^{fl/fl} Krt14-Cre* (G) mice contained a single cervical loop (arrow) from which a normally shaped maxillary incisor grew. In old *Atg7^{fl/fl} Krt14-Cre* (H) an additional cervical loop had formed, giving rise to an ectopic incisor. Scale bars: 200 μm.

macroscopic inspection as well as by micro-computed tomography (micro-CT) analysis (Figure 3A, D). Micro-CT analysis revealed that ectopic incisor tubes were present inside the primordial maxillary incisors in old *Atg7^{fl/fl} Krt14-Cre* (Figure 3E) but not *Atg7^{fl/fl}* mice (Figure 3B, C; Figure S4). These aberrant tubular structures were not present in young *Atg7^{fl/fl} Krt14-Cre* mice (Figure S5), indicating that they formed during aging. Histological investigation by hematoxylin and eosin staining showed aberrant structures of the cervical loop, i.e. the stem cell compartment of the maxillary incisors (Figure 3F–H) in aging *Atg7^{fl/fl} Krt14-Cre* mice (Figure 3H; Figure S6). Specifically, the lack of autophagy in epithelial cells resulted in the aberrant development of 2 or more cervical loops (Figure 3H; Figure S6), which

explained the growth of ectopic incisors and malformations of the front of the maxillary incisors. Thus, our results show that autophagy is required for the maintenance of a normal growth pattern of maxillary incisors during aging. Accordingly, *Atg7^{fl/fl} Krt14-Cre* mice represent a highly relevant model for future studies on the role of autophagy during the aging of dental epithelial stem cells.

Discussion

The results of this study demonstrate essential roles of autophagy in the rodent incisor model of amelogenesis and tooth growth. Suppression of ATG7-dependent autophagy in epithelial cells was compatible with the formation of enamel, however, the

secretion of iron in the final stages of amelogenesis on incisors was abrogated in the absence of autophagy. The additional phenotype of misshapen cervical loops and maxillary incisors in *Atg7^{fl/fl} Krt14-Cre* mice suggests a second role of autophagy in the control of epithelial stem cells and possibly in signaling to non-epithelial cells. While previous reports have suggested critical roles of autophagy in the response to extrinsic factors [22–24], this study indicates that autophagy is required for normal murine tooth biology.

At the cellular level, the deletion of *Atg7* resulted in the abrogation of GFP-LC3-labeled vesicles, accumulation of SQSTM1 and diffuse accumulation of iron in ameloblasts. With regard to the accumulation of SQSTM1 in the absence of ATG7, ameloblasts differ from epidermal keratinocytes and oral epithelial cells which do not, or only weakly, accumulate SQSTM1 in *Atg7^{fl/fl} Krt14-Cre* mice [16]. By contrast, ameloblasts resemble epithelial cells within the secretory portions of sweat glands and salivary glands of *Atg7^{fl/fl} Krt14-Cre* mice which accumulate SQSTM1 aggregates [19]. Of note, ameloblasts and secretory epithelial cells of sweat glands and salivary glands share a switch from expression of KRT5 and KRT14 to KRT8 and KRT18 during development, and they stop proliferation before initiating secretion. Together with previous reports, the results of this study indicate that epithelial cells in secretory organs have an elevated requirement for autophagy to maintain homeostasis, as compared to stratified non-secretory epithelial cells.

Autophagy was reported to contribute to secretion processes in osteoclasts and other cells [25–27]. In ameloblasts, the secretion of the main mass of the enamel is not impaired by *Krt14-Cre*-mediated deletion of *Atg7*, as evidenced by the micro-CT analysis of *Atg7^{fl/fl} Krt14-Cre* mouse teeth. The failure to form yellow incisors rather suggests that ATG7 is specifically required for the secretion of iron. The enamel epithelium of the maxillary incisors contains higher levels of ferritin, the intracellular iron storage complex, than any other tissue of mice [7]. Ferritin is a known substrate of lysosomal degradation via ferritinophagy mediated by the ferritin-binding protein NCOA4 (nuclear receptor coactivator 4) [28]. Ferritinophagy can release iron bound in ferritin for use by the cell or export. However, mice deficient of NCOA4 have yellow incisors (Fig. S7), suggesting that iron is exported from ameloblasts in an NCOA4-independent manner. Our data support the hypothesis that ameloblasts do not utilize NCOA4-dependent ferritinophagy but a separate ATG5- and ATG7-dependent ferritin degradation and iron secretion mechanism [29,30]. Interestingly, the deletion of *Atg5* was reported to cause transcriptional downregulation of the iron export channel, ferroportin, and iron deficiency in mice [31]. The mechanism of this dysregulation is not known yet, but it may also be activated by suppression of autophagy in ameloblasts and contribute to the blockade of iron secretion from the enamel epithelium of *Atg7^{fl/fl} Krt14-Cre* mice.

Besides the impairment of iron secretion, the growth of maxillary incisor of *Atg7^{fl/fl} Krt14-Cre* mice was altered during aging. Old *Atg7^{fl/fl} Krt14-Cre* mice developed severe odontoma-like malformations that, to the best of our knowledge, differ from incisor defects reported previously [32,33]. The hyperplasia of incisors in *Atg7^{fl/fl} Krt14-Cre* mice is probably not a secondary effect of iron deficiency in the enamel because other mouse lines

with iron-deficient incisors, such as *nfe2l2/nrf2* knockout mice [6], maintain normal tooth shape until an age of 2 years (Fig. S8). Histological data suggest that the malformations of *Atg7^{fl/fl} Krt14-Cre* incisors are a consequence of an as-yet unknown defect in the cell proliferation compartment of the incisor enamel epithelium, i.e. the cervical loop. While the spatial distribution of proliferating cells was normal in cervical loop of young *Atg7^{fl/fl} Krt14-Cre* mice (Fig. S9), it remains to be determined to what extent the rate of proliferation was altered by the absence of autophagy. Cell proliferation in the cervical loop is subjected to complex control mechanisms some of which have been linked to autophagy in other organs [34–38]. Further studies are required to determine the mechanism of growth dysregulation and to explore the possible use of *Atg7^{fl/fl} Krt14-Cre* incisors as a model for aging-associated tissue hyperplasia.

In conclusion, autophagy is essential for 2 independent processes in the enamel epithelium of murine incisors, i.e. the secretion of iron and the control of tissue homeostasis during aging.

Materials and methods

Mice

Mice were maintained in the animal facility of the Center of Translational Research, Medical University of Vienna. Breeding and genotyping of mice were done according to published protocols [14,16]. The following mouse strains were investigated: *Atg7^{fl/fl} Krt14-Cre* [14], *Atg7^{fl/fl} Krt14-Cre GFP-LC3* [14], *Atg5^{fl/fl} Krt5-Cre* [15], *nfe2l2/nrf2^{-/-}* [6], *sqstm1^{-/-}* [39], *CMV-Cre Ncoa4^{fl/fl}* [40]. Animal procedures were performed under approval by the Ethics Review Committee for Animal Experimentation of the Medical University of Vienna, Austria and the Federal Ministry of Science, Research and Economy, Austria (approval numbers BMWFW-66.009/0123-II/10b/2010 and BMWFW-66.009/0174-WF/V/3b/2017). *Ncoa4^{fl/fl} CMV-Cre* and *Ncoa4^{fl/fl}* mice [40] were generated and procedures were performed under the Dana-Farber Cancer Institute IACUC approved protocol (DFCI 15–020).

Histology, histochemistry and immunofluorescence labeling

Jaws of mice were fixed in formaldehyde, decalcified in EDTA solution (Gatt-Koller, 403,212,270), embedded in paraffin and sectioned at 1 or 3 μ m thickness through incisors. The sections were stained with hematoxylin (Merck, 1.09253.0500) and eosin (Sigma-Aldrich, 318,906) and Perls' Prussian blue (Dako, AR158) or subjected to immunolabeling. Immunohistochemical staining was performed by subsequent incubations with rabbit polyclonal anti-SQSTM1/p62 (MBL, PM045; dilution 1:1000) or rabbit anti-FTH1 (ferritin heavy polypeptide 1; LSBio, LS-B5847; 1:100), biotinylated anti-rabbit immunoglobulin G, affinity purified, made in goat (Vector Laboratories, BA-1000; 1:100) and Vectastain ABC horseradish peroxidase kit (Vector Laboratories, PK4000). Immunofluorescence labeling was performed with the primary antibodies rabbit anti-GFP (Abcam, ab290; 1:500), rabbit anti-MKI67/Ki67 (Abcam, ab15580; 1:500), and rat monoclonal anti-LGALS3/Mac-2 (lectin, galactose binding, soluble 3;

clone M3/38; Cedarlane, CL8942AP; 1:200) and the secondary antibodies goat anti-rabbit immunoglobulin conjugated to Alexa Fluor 488 (Invitrogen Molecular Probes, A11034; 1:500) and goat anti-rat immunoglobulin antibody conjugated to Alexa Fluor 546 (Invitrogen Molecular Probes, A11081; 1:500) according to published protocols [14,15,19]. Nuclei were counterstained with hematoxylin for immunohistochemistry and with Hoechst 33,258 (Molecular Probes, H1398) for immunofluorescence analysis. Isotype antibodies were used instead of the primary antibodies in negative control experiments. The immunolabeled sections were inspected with an Olympus AX 70 microscope (Hamburg, Germany) and photographed with a Spot RT3 slider camera (SPOT Imaging Solutions, Sterling Heights, MI, USA) and the imaging software Metamorph (Visitron Systems, Puchheim, Germany).

Micro-Computed Tomography (CT)

Micro-CT at a resolution of 10.0 μm was carried out using a $\mu\text{CT}35$ (SCANCO Medical AG, Brüttsellen, Switzerland). The scanning of the skulls was done at 70 kV/114 μA with an integration time of 500 ms. 3D volume renderings of the skulls were generated by Amira (Version 6.0.1, Visage Imaging Inc., San Diego, CA). A gray value threshold of about 1500 Hounsfield units (gray values range: $-6684 - 15,614$) was used to distinguish bone and tooth tissue from surrounding soft tissues. Frontal slices through teeth and bone tissue were produced. Images were taken using the Amira screenshot tool.

Statistical analysis

The numbers of ectopic incisor tubes were compared by the 2-tailed t-test with a *P*-value <0.05 being considered significant.

Acknowledgments

The authors thank Dr. Masaaki Komatsu (Tokyo Metropolitan Institute of Medical Science, Japan), Dr. Noboru Mizushima (Tokyo Medical and Dental University, Japan), Dr. Masayuki Yamamoto (University of Tsukuba, Japan), and Dr. Erwin F. Wagner (Medical University of Vienna, Austria) for providing genetically modified mice, and Dr. Jan Krivanek, Dr. Igor Adameyko, and Dr. Beate Lichtenberger (Medical University of Vienna, Austria) for helpful comments. We also thank Sophie Bergmann, Kinga Pajdzik, Bahar Golabi, Ionela Mariana Nagelreiter (Medical University of Vienna, Austria), and Dr. Naiara Santana Codina (Dana-Farber Cancer Institute, Boston, MA) for technical support. LE and FG acknowledge support from the TRANSAUTOPHAGY COST Action, CA15138.

Disclosure statement

No potential conflict of interest was reported by the authors.

Funding

JDM acknowledges support from the Burroughs Wellcome Fund Career Award for Medical Scientist, 1014767.

ORCID

Supawadee Sukseree <http://orcid.org/0000-0002-7011-9352>
 Uwe Yacine Schwarze <http://orcid.org/0000-0002-8954-0024>
 Reinhard Gruber <http://orcid.org/0000-0001-5400-9009>
 Florian Gruber <http://orcid.org/0000-0003-1094-5641>
 John D. Bartlett <http://orcid.org/0000-0003-2052-6299>
 Erwin Tschachler <http://orcid.org/0000-0002-0248-1798>
 Leopold Eckhart <http://orcid.org/0000-0002-5645-2036>

References

- [1] Smith CE. Cellular and chemical events during enamel maturation. *Crit Rev Oral Biol Med.* 1998;9:128–161.
- [2] Bartlett JD, Simmer JP. Proteinases in developing dental enamel. *Crit Rev Oral Biol Med.* 1999;10:425–441.
- [3] Møinichen CB, Lyngstadaas SP, Risnes S. Morphological characteristics of mouse incisor enamel. *J Anat.* 1996;189:325–333.
- [4] Wen X, Paine ML. Iron deposition and ferritin heavy chain (Fth) localization in rodent teeth. *BMC Res Notes.* 2013;6:1.
- [5] Gordon LM, Cohen MJ, MacRenaris KW, et al. Dental materials. Amorphous intergranular phases control the properties of rodent tooth enamel. *Science.* 2015;347:746–750.
- [6] Yanagawa T, Itoh K, Uwayama J, et al. Nrf2 deficiency causes tooth decolorization due to iron transport disorder in enamel organ. *Genes Cells.* 2004;9:641–651.
- [7] Miyazaki Y, Sakai H, Shibata Y, et al. Expression and localization of ferritin mRNA in ameloblasts of rat incisor. *Arch Oral Biol.* 1998;43:367–378.
- [8] Mizushima N, Komatsu M. Autophagy: renovation of cells and tissues. *Cell.* 2011;147:728–741.
- [9] Rogov V, Dötsch V, Johansen T, et al. Interactions between autophagy receptors and ubiquitin-like proteins form the molecular basis for selective autophagy. *Mol Cell.* 2014;53:167–178.
- [10] Choi AM, Ryter SW, Levine B. Autophagy in human health and disease. *N Engl J Med.* 2013;368:651–662.
- [11] Komatsu M, Waguri S, Ueno T, et al. Impairment of starvation-induced and constitutive autophagy in Atg7-deficient mice. *J Cell Biol.* 2005;169:425–434.
- [12] Hara T, Nakamura K, Matsui M, et al. Suppression of basal autophagy in neural cells causes neurodegenerative disease in mice. *Nature.* 2006;441:885–889.
- [13] Li H, Li D, Ma Z, et al. Defective autophagy in osteoblasts induces endoplasmic reticulum stress and causes remarkable bone loss. *Autophagy.* 2018;14:1726–1741.
- [14] Sukseree S, Mildner M, Rossiter H, et al. Autophagy in the thymic epithelium is dispensable for the development of self-tolerance in a novel mouse model. *PLoS One.* 2012;7:e38933.
- [15] Sukseree S, Rossiter H, Mildner M, et al. Targeted deletion of Atg5 reveals differential roles of autophagy in keratin K5-expressing epithelia. *Biochem Biophys Res Commun.* 2013;430:689–694.
- [16] Rossiter H, König U, Barresi C, et al. Epidermal keratinocytes form a functional skin barrier in the absence of Atg7 dependent autophagy. *J Dermatol Sci.* 2013;71:67–75.
- [17] Fischer H, Fumicz J, Rossiter H, et al. Holocrine secretion of sebum is a unique DNase2-dependent mode of programmed cell death. *J Invest Dermatol.* 2017;137:587–594.
- [18] Sukseree S, Bergmann S, Pajdzik K, et al. Suppression of autophagy perturbs turnover of sequestosome-1/p62 in Merkel cells but not in keratinocytes. *J Dermatol Sci.* 2018;90:209–211.
- [19] Sukseree S, Bergmann S, Pajdzik K, et al. Suppression of epithelial autophagy compromises the homeostasis of sweat glands during aging. *J Invest Dermatol.* 2018;138:2061–2063.
- [20] Duverger O, Ohara T, Shaffer JR, et al. Hair keratin mutations in tooth enamel increase dental decay risk. *J Clin Invest.* 2014;124:5219–5224.
- [21] Mizushima N, Yamamoto A, Matsui M, et al. In vivo analysis of autophagy in response to nutrient starvation using transgenic mice expressing a fluorescent autophagosome marker. *Mol Biol Cell.* 2004;15:1101–1111.

- [22] Suzuki M, Bartlett JD. Sirtuin1 and autophagy protect cells from fluoride-induced cell stress. *Biochim Biophys Acta*. 2014;1842:245–255.
- [23] Suzuki M, Bandoski C, Bartlett JD. Fluoride induces oxidative damage and SIRT1/autophagy through ROS-mediated JNK signaling. *Free Radic Biol Med*. 2015;89:369–378.
- [24] Zhuang H, Ali K, Ardu S, et al. Autophagy in dental tissues: a double-edged sword. *Cell Death Dis*. 2016;7:e2192.
- [25] Deretic V, Jiang S, Dupont N. Autophagy intersections with conventional and unconventional secretion in tissue development, remodeling and inflammation. *Trends Cell Biol*. 2012;22:397–406.
- [26] DeSelm CJ, Miller BC, Zou W, et al. Autophagy proteins regulate the secretory component of osteoclastic bone resorption. *Dev Cell*. 2011;21:966–974.
- [27] Ponpuak M, Mandell MA, Kimura T, et al. Secretory autophagy. *Curr Opin Cell Biol*. 2015;35:106–116.
- [28] Mancias JD, Wang X, Gygi SP, et al. Quantitative proteomics identifies NCOA4 as the cargo receptor mediating ferritinophagy. *Nature*. 2014;509:105–109.
- [29] Asano T, Komatsu M, Yamaguchi-Iwai Y, et al. Distinct mechanisms of ferritin delivery to lysosomes in iron-depleted and iron-replete cells. *Mol Cell Biol*. 2011;31:2040–2052.
- [30] Goodwin JM, Dowdle WE, DeJesus R, et al. Autophagy-independent lysosomal targeting regulated by ULK1/2-FIP200 and ATG9. *Cell Rep*. 2017;20:2341–2356.
- [31] Yoshii SR, Kuma A, Akashi T, et al. Systemic analysis of Atg5-null mice rescued from neonatal lethality by transgenic ATG5 expression in neurons. *Dev Cell*. 2016;39:116–130.
- [32] Charles C, Hovorakova M, Ahn Y, et al. Regulation of tooth number by fine-tuning levels of receptor-tyrosine kinase signaling. *Development*. 2011;138:4063–4073.
- [33] Blackburn J, Kawasaki K, Porntaveetus T, et al. Excess NF- κ B induces ectopic odontogenesis in embryonic incisor epithelium. *J Dent Res*. 2015;94:121–128.
- [34] Sharir A, Marangoni P, Zilionis R, et al. A large pool of actively cycling progenitors orchestrates self-renewal and injury repair of an ectodermal appendage. *Nat Cell Biol*. 2019;21:1102–1112.
- [35] Binder M, Chmielarz P, Mckinnon PJ, et al. Functionally distinctive Ptch receptors establish multimodal hedgehog signaling in the tooth epithelial stem cell niche. *Stem Cells*. 2019;37:1238–1248.
- [36] Xavier GM, Patist AL, Healy C, et al. Activated WNT signaling in postnatal SOX2-positive dental stem cells can drive odontoma formation. *Sci Rep*. 2015;5:14479.
- [37] Hu JK, Du W, Shelton SJ, et al. An FAK-YAP-mTOR signaling axis regulates stem cell-based tissue renewal in mice. *Cell Stem Cell*. 2017;21:91–106.
- [38] Lee YA, Noon LA, Akat KM, et al. Autophagy is a gatekeeper of hepatic differentiation and carcinogenesis by controlling the degradation of Yap. *Nat Commun*. 2018;9:4962.
- [39] Komatsu M, Waguri S, Koike M, et al. Homeostatic levels of p62 control cytoplasmic inclusion body formation in autophagy-deficient mice. *Cell*. 2007;131:1149–1163.
- [40] Santana-Codina N, Gableske S, Quiles Del Rey M, et al. NCOA4 maintains murine erythropoiesis via cell autonomous and non-autonomous mechanisms. *Haematologica*. 2019;104:1342–1354.